

MSc Mathematics
Track: Biomedical Mathematics

Master thesis

Mathematical model of orientation in insects brain

by
Francesca Candelora

July 7, 2022

Supervisor: prof.dr. Daniele Avitabile
Second examiner: prof. dr. Chris Bick

Department of Mathematics
Faculty of Sciences



Abstract

Orientation in animals is based on two mechanisms, landmark navigation and path integration. They rely on externally and internally available information to encode compass direction and store memory about performed paths. Since in fly's brain these mechanisms work through bumps of activity, we propose two biophysically inspired models based on neural field theory. The model for landmark navigation reproduces a bump in the fly's ellipsoid body, able to follow external inputs with a smoothing effect. To some extent it can follow abrupt variations of the position of external inputs. We produce a bifurcation diagram to see how some characteristics of the input can influence the eventual jumps of the activity bump. The second model is about path integration. We want to model the ability of a tethered fly to return back to an initial position after an outbound route. In order to do this we construct a model based on biological evidence, considering the connectivity of three populations in the fly's central complex. The so produced model is always able to return back in the correct direction towards an initial position, even after some oscillations. However, its capability of reaching the initial position is highly influenced by the memory decay component. Future expansion of this research could be to implement the same model in a 2D environment, including other populations of neurons which encode spatial information.

Title: Mathematical model of orientation in insects brain
Author: Francesca Candelora, f.candelora@vu.nl, 2669778
Supervisor: prof.dr. Daniele Avitabile
Second examiner: prof. dr. Chris Bick
Date: July 7, 2022

Department of Mathematics
VU University Amsterdam
de Boelelaan 1081, 1081 HV Amsterdam
<http://www.math.vu.nl/>

Contents

1	Introduction	5
2	Neural fields theory	9
2.1	Definition of model	9
2.2	Homogeneous steady states	10
2.3	Bump construction	13
3	Landmark navigation	18
3.1	Discretization of neural field	18
3.2	Results of simulations	20
3.3	Input jumps and bifurcation analysis	23
4	Path integration	27
4.1	Description of the biological network	27
4.2	Mathematical modelling of the network	29
4.3	Results of input application	33
5	Conclusions	37

Acknowledgements

First of all, I would like to thank Daniele, the most caring professor I met. Thank you for encouraging me and keeping me motivated even when I wanted to give up. Thanks to Chris for his support and interest.

I would like to dedicate this work to all the people who have been with me during this years.

To my sister Chiara, you are special, I never tell you enough how much I love you.

To my parents, who encourage me to be the person I want to be.

To Ilaria, who guides me through the hard path of knowing who I am.

To my housemates Fla, Fra, Liu and Genni, you are the softest.

To the Suore, you are the best friends I have.

To Noems, for your loyalty and your willingness to explore.

To Sara, for being a companion in my craziness.

To Raffa, reminding me how lucky I am to know such a wonderful person.

To Lu, "sometimes apart but never at heart".

To Franci, who taught me the importance of taking my time.

To all my friends who I haven't named here.

Thanks for being part of who I am today.

1 Introduction

The orientation of animals in space relies on both external (allothetic) and internal (idiothetic) cues. The two mechanisms taking place in animals brain that process this information are respectively landmark navigation and path integration, which simultaneously integrate the external and the self-motion cues [20]. Landmark navigation processes information coming from the environment, even though cerebral areas involved are not directly connected to sensory inputs. On the other side, idiothetic cues consisting of internally available information about position and orientation are constantly processed in path integration in order for the animal to update its position.

Landmark navigation and path integration in *Drosophila melanogaster* are operated in the central complex (CX), a high-order neuropil that integrates sensory and motor information, relaying it to motor control centers [10, 17]. The CX consists in different areas located next to each other in the *Drosophila* brain: the ellipsoid body (EB), the fan shaped body (FB), the protocerebral bridge (PB), the galls (GA), the noduli (NO), all made of interconnected columnar neurons [10, 18]. A stylized image of the CX can be found in figure 1.1.

There are two different kinds of columnar neurons connecting the EB and PB: E-PG and P-EN neurons, represented in figure 1.2. E-PG neurons encode internal heading direction, and have dendritic arbors in the EB, outputting in both galls and PB. Every E-PG neuron in the EB connected to either side of the PB neighbors two E-PG neurons connected to the other side, see figure 1.3 to the left. For example, the yellow wedge is connected to the yellow glomerulus in the right PB. Its neighbors are the dashed yellow and dashed orange wedges, both of which are connected to glomeruli in the left PB. This way, when there is a peak of activity in one of the 16 wedges, a smaller amount of activity is registered in the neighboring ones, and they represent stimuli coming from the same direction in which the fly is pointing. P-EN neurons, called “shifting neurons”, instead, have dendritic arbors in the PB and output in the EB and NO [4, 18]. Every “tile” in the EB (overlapping two wedges) is innervated by two different glomeruli in the PB, one from the right and one from the left side, see figure 1.3. These neurons are responsible

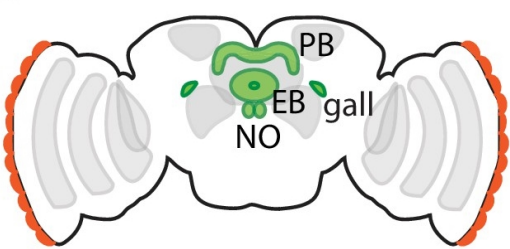


Figure 1.1: Visualization of the *Drosophila*'s brain, in grey. The green colored parts compose the central complex (CX): PB, EB, NO and galls; FB is not highlighted. In red, position of the eyes. Picture adapted from [22]

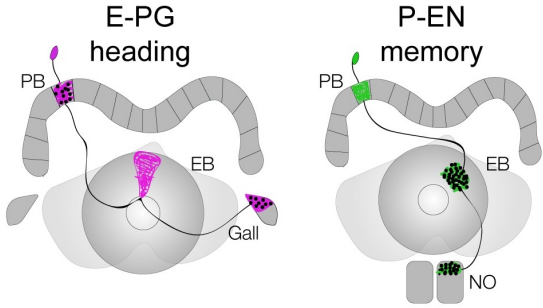


Figure 1.2: Visualization of E-PG and P-EN neurons. E-PG (pink) have dendrites in the EB and output in PB and Galls, they encode head direction. P-EN (green) have dendrites in PB outputting in EB and Noduli. They encode memory. Picture adapted from [18].

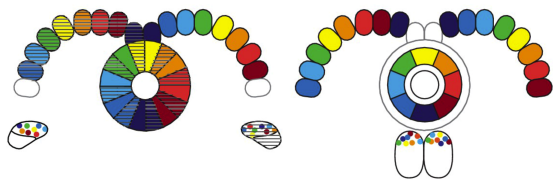


Figure 1.3: Tiling of EB and PB by E-PG and P-EN neurons. E-PG neurons divide the EB in 16 wedges, and each is connected to one glomeruli in PB. P-EN neurons divide the EB in 8 tiles and each receives input from two glomeruli in PB. Picture adapted from [22]

of keeping track of the memory of the animal’s journeys, receiving information about whether changes of direction happen clockwise or counterclockwise and at which speed.

Landmark navigation is mainly executed by head-direction (HD) cells, a family of neurons encoding, at any point in time, the direction where the head is pointing with respect to some landmark cues. It has been shown that these cells disregard the position of the trunk and any pitch or roll movement up to 90° from the horizontal plane [20]. Every HD cell only fires when the head of the animal is pointing in a range of directions that is specific for that cell. The direction at which the cells have their maximum firing rate - the peak firing rate - is referred to as the preferred direction [20]. Firing of HD cells is unaffected by the behavior of the animal: no matter what the animal is doing, even during sleep or when it is mechanically moved, these cells always signal the head direction [21].

Since the preferred direction is relative to the external environment, there are exper-

Table of acronyms

CX	Central Complex
FB	Fan-shaped Body
EB	Ellipsoid Body
PB	Protocerebral Bridge
NO	Noduli
GA	Galls
HD	Head Direction

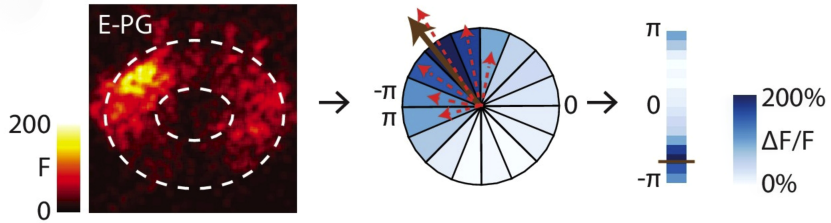


Figure 1.4: A bump in HD cells (left) registered with a two-photon imaging technique. Lighter colors represent higher activity, the area with highest activity represent the head direction. To the right, a schematic representation of the fly’s HD. Picture adapted from [22].

iments showing that in familiar and unambiguous environments the preferred direction of HD cells remains the same for days [15]. In such a case neighbouring HD cells conserve the same relative preferred direction, however not necessarily two adjacent cells fire at adjacent directions. For simplicity, when modelling networks of HD cells as ring attractors, cells representing adjacent preferred directions are located next to each other [15]. These networks encode the compass direction through a bump of activity, that dynamically tracks movements of the fly’s head, thus mapping the space in the central complex [10, 17]. Since the strongest directional input contributes most to the bump peak, this represents the direction of the animal, see figure 1.4.

The EB is a network of HD cells topologically arranged on a toroidal structure, subdivided in tiled domains, any of which is connected to one or two glomeruli in the PB, depending on their function [10]. For simplicity, since only the angular direction of neurons matters for our purposes, we are going to consider the torus as a ring domain. It has been demonstrated that ring attractor networks are very effective in modelling networks of head direction cells [6, 9, 12, 16, 20, 24]. A ring attractor structure is possible due to an internally organization of inhibitory recurrent connections between neurons [12], which is going to be explained more deeply in chapter 3.

Neurons in the PB, instead, integrate information about the animal’s heading by controlling movements in the clockwise and counterclockwise directions [4, 10]. These neurons act as an activity-based memory, constructed by constantly integrating information from the movement of the animal [17], resulting in a bump of activity such as the one found in EB.

It has been shown that the above discussed mechanisms allow a fly to recover its initial position in space, after performing an outbound journey [17]. Purpose of this work is to build a mathematical model that behaves such as the fly does, when orienting in space. Neural fields are going to be the outlying mathematics to the model, as discussed in chapter 2. We are going to present a general introduction of neural fields, together with a bump construction and discussion about stability. Since we wish to model discretized domain we are defining a discretized version of neural fields, and in order to study it we are borrowing results from the continuous limit theory. We are performing simulations of the behavior of a tethered fly in a visual arena. The fly is kept at the center of a cylindrical LED screen, which is going to be turned on only for a narrow vertical bar that rotates around the arena. Our first experiment, in chapter 3 consists in modeling the HD cells in the EB as a discretized neural field, in order to see a bump of activity. We show that this bump follows the movements of the vertical bar (the external input) in the LED arena, behaving similarly as the bump of activity in the fly's brain.

We are also interested in the so called "jumps" [6]. There are, in fact, cases when the bump moves abruptly from its position to another in the domain, when an input is suddenly moved of a certain angle, following the input. This is not always the case. If the input is not strong or narrow enough, the bump keeps flowing until it reaches the input position, with some delay. Thus, it was interesting to make a bifurcation diagram for input jumping of fixed angles. It is reported in section 3.3.

The second experiment performed, in chapter 4 is about home returning from outbound routes. In fact, it has been shown that the mechanisms in the CX allow insects to return directly (almost linearly) to their initial position, after they have performed journeys in space. This behavior is going to be modelled using neural fields on a network of recurrent connections between three populations in the fly's CX. Again, this model is applied on a tethered fly, in a 1D environment. In all the experiments performed the fly was always able to go back in the correct direction, towards the initial position, although it was not always the case that the fly could reach that position.

We wanted to model the architecture of the fly's brain with the smallest possible amount of variables. We managed to do so using three populations of neurons, which are sufficient for a 1D setting. However, in order to model movements of the fly in a 2D environment, populations encoding spatial information, like neurons in the noduli, need to be included in the model.

2 Neural fields theory

Neural field theory has been developed to describe populations of neurons when the behavior (spiking or firing rate) of the single neuron is not as important as the behavior of the population itself. In particular, one treats a population of neurons as a continuum field of which the level of activity is computed [3]. There are several versions of neural field models. They differ on their dynamics behavior - for example periodic patterns or bumps of activity could arise, or travelling wave patterns can be sustained [2, 7, 13, 19] - or in the way populations are treated. When there are both inhibitory and excitatory populations, one could describe them separately, using Wilson-Cowan equations [23]. Since in this case we are more interested in the response of the population - whose neurons are inhibitory and excitatory at the same time - as a whole, we are going to incorporate information about excitatory and inhibitory connections inside the model itself, as it is going to be explained below, keeping the form of a single Wilson-Cowan equation. The model is going to be defined in section 2.1, then stability of the homogeneous stationary state is studied in section 2.2, and lastly, section 2.3 contains the construction and stability analysis of a localized steady state, using the Amari construction.

2.1 Definition of model

A bump of activity can be defined a localized excitation, that arises in a domain after applying a localized stimulus. We wish to build a model where a bump of activity travels in time and space as a response to certain stimuli, thus the spiking times and rates of single neurons are not relevant in our analysis. Therefore, we are using neural fields that are able to sustain a local bump of activity, such as it has been observed in biological studies on the fly [10]. It was also shown that the biological networks that we are going to model, have a ring attractor structure, mainly due to their connectivity [6, 9, 12, 16, 20, 24].

For simplicity the ring domain is transformed into the interval $\Omega = (-\pi, \pi]$, so that we have a single variable indicating the angle θ . Then, the evolutionary equation can be written as:

$$\partial_t u(\theta, t) = -u(\theta, t) + \int_{\Omega} w(\theta, \theta') f(u(\theta', t)) d\theta' + I(\theta, t)$$

In this model we have:

- $u(\theta, t)$, representing the activity at position $\theta \in \Omega$ and time $t > 0$;
- $w(\theta, \theta')$, called the “synaptic kernel”;

- $f(u(\theta, t))$, the firing rate function, which depends on the activity level $u(\theta, t)$, and
- $I(\theta, t)$ the external input applied at position θ at time t .

The synaptic kernel $w(\theta, \theta')$ is in general a function of two variables, representing the magnitude of connectivity between two points θ and θ' in the domain Ω . Since we are considering a population made of all identical cells, and the network connectivity is identical for all neurons, so we have both homogeneity and isotropy, we can consider there to be a ring symmetry. This enables us to define the angular difference

$$z := d(\theta, \theta') = \theta' - \theta$$

Using this distance, we can define w as a function of only one variable, z :

$$w(\theta, \theta') = W(\theta' - \theta) = W(z)$$

where W is a symmetric function $W : \Omega \rightarrow \mathbb{R}$. Using this function we can rewrite the equation of the model as an integral equation containing a convolution:

$$\partial_t u(\theta, t) = -u(\theta, t) + \int_{\Omega} W(\theta' - \theta) f(u(\theta', t)) d\theta' + I(\theta, t)$$

The choice of W depends on the connectivity of the network that is going to be modelled. In fact, $W(z) > 0$ indicates excitatory connection between any two neurons distanced of z and $W(z) < 0$ indicates inhibitory connection at distance z [1]. Apart for the network connectivity, there are no other motivations in deciding how to define W , except for simplicity in the computations. In particular, since we want to model a network with both inhibitory and excitatory connections we choose W as a “Mexican hat” function as follows:

$$W(z) = a_1 \exp(-b_1|z|) - a_2 \exp(-b_2|z|)$$

Moving on to the firing rate f , it is a function of the activity $u(\theta, t)$ bounded between 0 and 1, influencing patterns that can be sustained by the model. We define it as a sigmoid function,

$$f(u(\theta, t)) = \frac{1}{1 + \exp(-\mu(u - h))}$$

where the parameter h is the firing rate threshold and μ influences the steepness of the sigmoid. Depending on the choice of parameters, there can be several outcomes for the model. In fact the activity can be dampened, or some patterns of low or high activity can appear and be sustained with appropriate initial conditions.

2.2 Homogeneous steady states

In order to study homogeneous steady states of the system, we need to define some hypotheses:

H1. $I(\theta, t) \equiv 0$. For constant input, it is sufficient to rescale, otherwise no homogeneous steady states are allowed.

H2. $w(\theta, \theta') = W(\theta - \theta')$, $W(z)$ even and rapidly decaying, and $\int_{\Omega} W(z) dz = W_0 < \infty$. Suppose the homogeneous equilibrium is the constant $u(\theta, t) \equiv U \in \mathbb{R}$. Then, we can rewrite the model equation as

$$0 = -U + \int_{\Omega} W(\theta' - \theta) f(U) d\theta'$$

Since $f(U)$ does not depend on the angle variable θ anymore, we can take it out of the integral:

$$0 = -U + f(U) \int_{\Omega} W(\theta' - \theta) d\theta'$$

Using **H2.** we have a linear equation in U for homogeneous equilibria:

$$U = W_0 f(U)$$

where U is the fixed point of the map

$$U \mapsto W_0 f(U)$$

This equation can either have one or three solutions, as depicted in figure 2.1.

We are now going to study the stability of such equilibria. In order to do so, we are going to perturb the steady state by a small amount $\tilde{u}(\theta, t)$.

$$u(\theta, t) = U + \tilde{u}(\theta, t)$$

Then, the equation becomes

$$\partial_t(U + \tilde{u}(\theta, t)) = -(U + \tilde{u}(\theta, t)) + \int_{\Omega} W(\theta' - \theta) f(U + \tilde{u}(\theta', t)) d\theta'$$

Since the only nonlinear term is given by the function $f(u)$ in the integral, the linearization is going to be applied there. By using Taylor expansion, under the hypothesis that f is sufficiently regular - which is satisfied because a sigmoid is differentiable infinitely many times - and considering a perturbation v of u , we can write:

$$f(u + v) = f(u) + f'(u)v + \mathcal{O}(v^2)$$

Thus, neglecting the term $\mathcal{O}(\|\tilde{u}(\theta, t)\|)$,

$$\partial_t \tilde{u}(\theta, t) = -(U + \tilde{u}(\theta, t)) + \int_{\Omega} W(\theta' - \theta)(f(U) + f'(U)\tilde{u}(\theta', t)) d\theta'$$

Since $f(U)$ does not depend on θ , using **H2.** again, and since $f'(U)$ is a constant, we have:

$$\partial_t \tilde{u}(\theta, t) = -(U + \tilde{u}(\theta, t)) + f(U)W_0 + f'(U) \int_{\Omega} W(\theta' - \theta)\tilde{u}(\theta', t) d\theta'$$

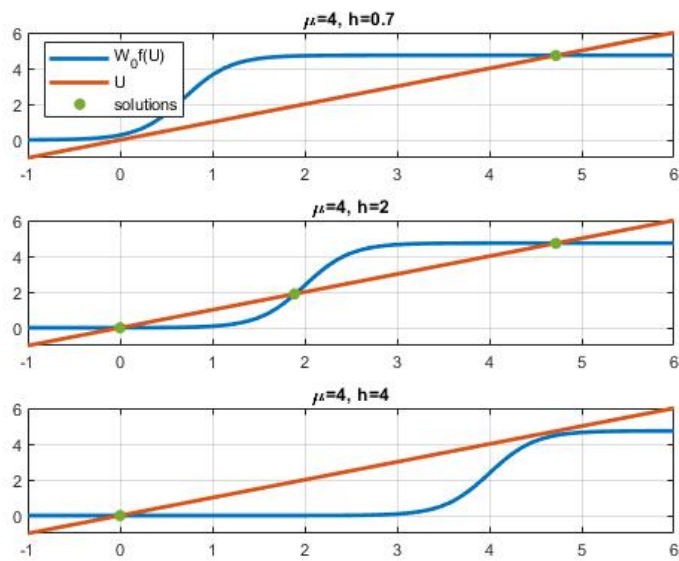


Figure 2.1: Graphs of $W_0 f(U)$ against U for three choices of μ and h , with parameters $a_1 = 30$ $b_1 = 5$ $a_2 = 5.5$ $b_2 = 1.5$. $W_0 = \int_{\Omega} W(\theta' - \theta) d\theta$, $W(z) = a_1 \exp(-b_1|z|) - a_2 \exp(-b_2|z|)$, $f(U) = \frac{1}{1 + \exp(-\mu(U-h))}$. The first and last figures have one possible solution to the equation $U = W_0 f(U)$, while the second one has three possible solutions.

Then, since U is a steady state, it still holds $U = W_0 f(U)$, so the equation simplifies to:

$$\partial_t \tilde{u}(\theta, t) = -\tilde{u}(\theta, t) + f'(U) \int_{\Omega} W(\theta' - \theta) \tilde{u}(\theta', t) d\theta'$$

This equation does not contain the nonlinearity of f anymore. We want, then, to find solutions to the problem:

$$\begin{cases} \partial_t \tilde{u}(\theta, t) &= -\tilde{u}(\theta, t) + f'(U) \int_{\Omega} W(\theta' - \theta) \tilde{u}(\theta', t) d\theta' \\ \tilde{u}(\theta, 0) &= \tilde{u}_0(\theta) \end{cases} \quad (2.1)$$

The last integral is a convolution between W and \tilde{u} . In order to find solutions to the problem 2.1, we use Fourier transformations to the wavelength space and then transform back, because studying the transformed version of this problem is mathematically easier. Denoting by $\hat{u}(k, t)$ the Fourier transform of $u(\theta, t)$ in the variable θ , we can write:

$$\begin{cases} \partial_t \hat{u}(k, t) &= -\hat{u}(k, t) + f'(U) \hat{W}(k) \hat{u}(k, t) \\ \hat{u}(k, 0) &= \hat{u}_0(k) \end{cases}$$

Defining $\lambda(k) := -1 + f'(U) \hat{W}(k)$, a simpler form of this problem can be written:

$$\begin{cases} \partial_t \hat{u}(k, t) &= \lambda(k) \hat{u}(k, t) \\ \hat{u}(k, 0) &= \hat{u}_0(k) \end{cases}$$

And since solutions to this problem are of the form

$$\hat{u}(k, t) = \hat{u}_0(k) \exp(\lambda(k)t)$$

we can apply the inverse Fourier transformation to these solutions to find solutions of 2.1:

$$\tilde{u}(\theta, t) = \int_{\Omega} \hat{u}_0(k) \exp(\lambda(k)t) \exp(2\pi i k \theta) dk$$

Stability of these solutions can be derived by studying the sign of $\Re(\lambda(k))$, where \Re is the real part of a complex number. In fact, if $\Re(\lambda(k)) < 0$ perturbations get damped, if $\Re(\lambda(k)) > 0$ they get amplified, meaning that in the first case equilibria are stable and in the other one they are unstable. In particular, since $\lambda(k)$ were defined as $\lambda(k) = -1 + f'(U) \hat{W}(k)$ the stability of equilibria depends on the relation between $\hat{W}(k)$ and the inverse of $f'(U)$.

2.3 Bump construction

In the previous section we studied stability of homogeneous equilibria. With a slight modification, we can study the construction of a bump of activity in a neural field model

as a localized stationary state, and study its stability. In order to do that we consider again a neural field in absence of external stimulus, $I(\theta, t) \equiv 0$:

$$\partial_t u(\theta, t) = -u(\theta, t) + \int_{\Omega} W(\theta - \theta') f(u(\theta', t)) d\theta' \quad (2.2)$$

Then, we need to formulate an additional hypothesis:

H3. $\lim_{z \rightarrow \infty} W(z) = 0$.

This is the case because we are considering a Mexican hat function, whose parameters can be tuned to approach 0 at infinity. Then, since we wish to study localized stationary states, we want them to be of the form: $u(\theta, t) = U(\theta)$. Thus, the system can be written as

$$0 = -U(\theta) + \int_{\Omega} W(\theta - \theta') f(U(\theta')) d\theta' \quad (2.3)$$

Functional analysis tool can be used to prove existence of a solution $U(\theta)$ that satisfies the above equation. Amari showed that choosing the nonlinearity term f to be a Heaviside function, solutions to the problem can be found using pen and paper computations [1]. Then numerical approximation of the solution can be obtained for the case when f is a sigmoid [23]. However, we are not focusing on the existence of solutions, since we are interested in qualitative study of solutions themselves.

In order to study the linear stability of solutions $U(\theta)$ to perturbations $\tilde{u}(\theta, t)$, we need to make an hypothesis that perturbations are of the form

$$\tilde{u}(\theta, t) = \exp(\lambda t) V(\theta)$$

where $(\lambda, V(\theta))$ are eigenpairs of the stability problem

$$\lambda V(\theta) = -V(\theta) + \int_{\Omega} W(\theta - \theta') f'(U(\theta')) V(\theta') d\theta' \quad (2.4)$$

Equation 2.2 has an important property, that we are going to use in the future, namely rotation invariance. In fact, shifts in the variable θ leave the equation untouched. By defining the right hand side of the equation as an operator,

$$\mathcal{F}(u(\cdot, t))(\theta) := -u(\theta, t) + \int_{\Omega} W(\theta - \theta') f(u(\theta', t)) d\theta'$$

and imposing a spatial shift in the coordinate θ, θ_0 ,

$$\partial_t u(\theta + \theta_0, t) = -u(\theta + \theta_0, t) + \int_{\Omega} W(\theta + \theta_0 - \theta') f(u(\theta', t)) d\theta'$$

With a change of coordinates: $\theta' = \zeta + \theta_0$,

$$\partial_t u(\theta + \theta_0, t) = -u(\theta + \theta_0, t) + \int_{\Omega} W(\theta - \zeta) f(u(\zeta + \theta_0, t)) d\zeta \quad (2.5)$$

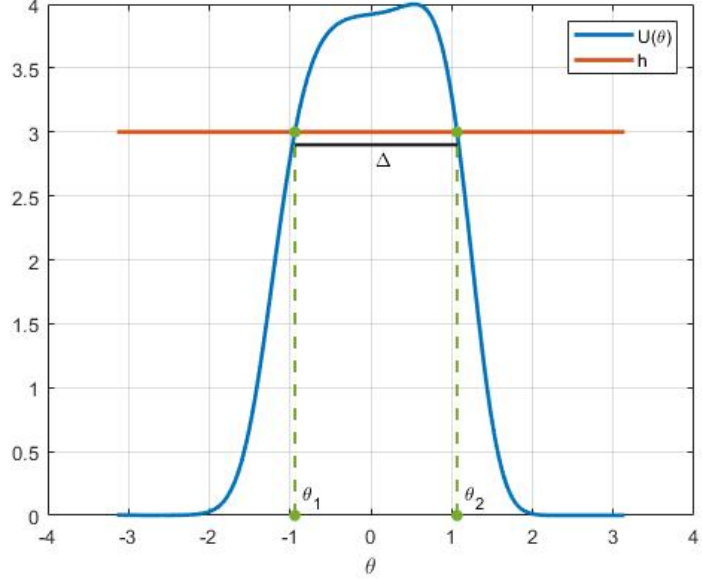


Figure 2.2: Example of a bump (blue line). The intersection with the threshold h is at θ_1 and θ_2 , which are the extremes of the compact interval A . The width of the bump is defined as $\Delta = \theta_2 - \theta_1$.

the solution has moved in space, and we found a new solution just by shifting the previous one, so by translation invariance. The right hand side of equation 2.5 can be written as $\mathcal{F}(u(\cdot + \theta_0, t))(\theta)$ or equivalently $\mathcal{F}(u(\cdot, t))(\theta + \theta_0)$.

There are two main consequences of translation invariance. First of all, any translation of a solution is still a solution, so we can find new solutions just by shifting the already existing ones by any constant θ_0 , without loss of generality. Secondly, if $U(\theta)$ is a stationary solution, up to translation invariance, then $(\lambda, V(\theta)) = (0, U'(\theta))$ is an eigenpair:

$$0 \cdot U'(\theta) = -U'(\theta) + \int_{\Omega} W(\theta - \theta') f(U'(\theta')) U'(\theta') d\theta' \quad (2.6)$$

In fact, if $U(\theta)$ is an equilibrium, equation 2.3 holds, and by differentiating it and using the chain rule we obtain 2.6.

By using the Amari construction [1], we suppose that the firing rate is a Heaviside function:

H4. $f(u) = H(u - h)$, where h is the threshold parameter.

Under this hypothesis we can define a localized bump, as a steady state such that $\lim_{\theta \rightarrow \pm\infty} U(\theta) = 0$, $U \in \mathcal{C}(\mathbb{R})$, and $U(\theta) \geq h$ for all $\theta \in A = [\theta_1, \theta_2]$, with A compact interval. The last property is the one that allows the bump of activity to be localized. We also define $\Delta = \theta_2 - \theta_1$ as the width of the bump, see figure 2.2 for an example.

When hypothesis **H4.** holds, the problem reduces to find the intersection points between $U(\theta)$ and h : $\{\theta_1, \theta_2\}$. In fact, under **H4.**, finding a localized bump is equivalent

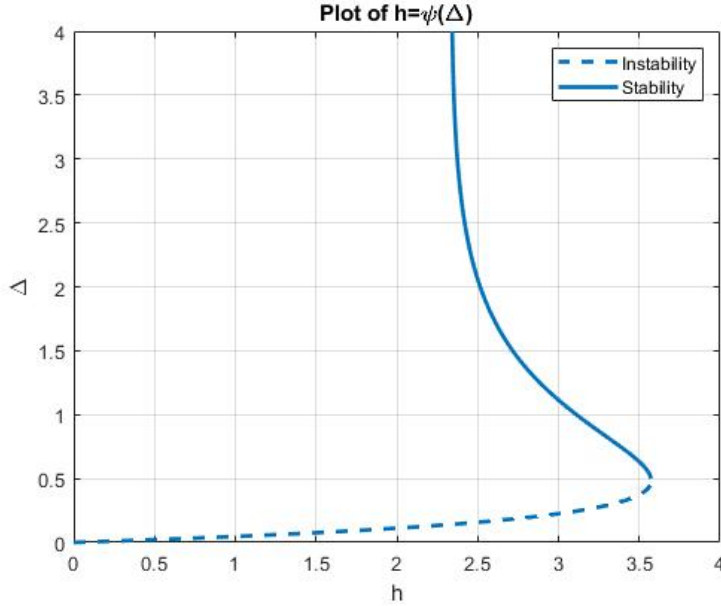


Figure 2.3: Bifurcation diagram showing the function $\psi(\Delta) = \int_0^\Delta W(\theta')d\theta'$. Parameters for W are $a_1 = 30$; $b_1 = 5$; $a_2 = 5.5$; $b_2 = 1.5$. The dashed line represents instability, while the continuous one represents stability of the localized solution.

to solving equation 2.3, which in this case reduces to

$$\begin{aligned} U(\theta) &= \int_{\Omega} W(\theta - \theta') H(U(\theta') - h) d\theta' \\ &= \int_A W(\theta - \theta') d\theta' \end{aligned}$$

because $U(\theta) \geq h$ (thus $H(U - h) = 1$) only on the interval A . Thus, if we know θ_1 and θ_2 we can construct $U(\theta)$ as

$$U(\theta) = \int_{\theta_1}^{\theta_2} W(\theta - \theta') d\theta'$$

We found that the shape of $U(\theta)$ depends on $W(z)$, once it is defined, and by evaluating $U(\theta)$ at θ_1 when it is equal to the threshold h , and applying a change of variable we can write

$$h = \int_0^\Delta W(\theta') d\theta'$$

This allows us to define an algorithm for constructing a bump. First of all, we need to find a pair (h, Δ) such that $h = \psi(\Delta)$, where ψ is the map

$$\psi : \Delta \mapsto \int_0^\Delta W(\theta') d\theta'$$

Then, by translation invariance we define $\theta_1 = 0$ and $\theta_2 = \Delta$. And lastly we can construct the bump using

$$U(\theta) = \int_0^\Delta W(\theta - \theta') d\theta' \quad (2.7)$$

Again, by translation invariance, the bump can be shifted anywhere in the domain Ω .

In order to study linear stability of the localized steady state $U(\theta)$, we recall the stability problem 2.4, which we can rewrite using **H4.** as follows

$$\lambda V(\theta) = -V(\theta) + \int_\Omega W(\theta - \theta') \delta(U(\theta') - h) V(\theta') d\theta'$$

where the symbol δ indicates the Dirac delta. By writing as θ_i , $i = 1, 2$ the two roots of $U(\theta) - h$, and using the property of the Dirac delta, we can write

$$\lambda V(\theta) = -V(\theta) + \int_\Omega W(\theta - \theta') \sum_{j=1}^2 \frac{\delta(\theta' - \theta_j)}{|U'(\theta_j)|} V(\theta') d\theta'$$

and thus

$$(\lambda + 1)V(\theta) = \sum_{j=1}^2 \left(\frac{W(\theta - \theta_j)}{|U'(\theta_j)|} V(\theta_j) \right).$$

Knowing λ , θ_j and $V(\theta_j)$, one can deduce the form of $V(\theta)$. In order to study the stability of equilibria, one can evaluate the equation at $\theta = \theta_i$, obtaining two equations, that can be written in a matrix form using the notation $V_j := V(\theta_j)$:

$$\lambda \begin{bmatrix} V_1 \\ V_2 \end{bmatrix} = \begin{bmatrix} -1 + \frac{W(0)}{|W(0)-W(\Delta)|} & \frac{W(\Delta)}{|W(0)-W(\Delta)|} \\ \frac{W(\Delta)}{|W(0)-W(\Delta)|} & -1 + \frac{W(0)}{|W(0)-W(\Delta)|} \end{bmatrix} \begin{bmatrix} V_1 \\ V_2 \end{bmatrix}$$

where the denominators come from the fundamental theorem of integral calculus, as U is somewhat defined as the primitive of W in equation 2.7. Thus, computing values of the matrix

$$M := \begin{bmatrix} -1 + \frac{W(0)}{|W(0)-W(\Delta)|} & \frac{W(\Delta)}{|W(0)-W(\Delta)|} \\ \frac{W(\Delta)}{|W(0)-W(\Delta)|} & -1 + \frac{W(0)}{|W(0)-W(\Delta)|} \end{bmatrix}$$

and its eigenpairs (λ, V) , then one can compute $V(\theta)$ using the relation

$$V(\theta) = \frac{1}{1 + \lambda} \sum_{j=1}^2 \left(\frac{W(\theta - \theta_j)}{|U'(\theta_j)|} V_j \right)$$

We showed before that one of the eigenvalues is $\lambda = 0$, with eigenfunction $V(\theta) = U'(\theta)$, which being null has no effect on the stability of the equilibrium. The other eigenvalue is purely real and can be either positive or negative, making the solution respectively unstable or stable, depending on where it falls in the bifurcation diagram, see figure 2.3.

In conclusion, in order to have a stable equilibrium as a bump of activity, one needs to set parameters such that $h = \psi(\Delta)$ falls in the upper branch of the bifurcation diagram in figure 2.3, by following the procedure described above.

3 Landmark navigation

The first experiment performed takes place in a LED arena, called virtual arena, which is made of a cylindrical LED screen in the middle of which a fly is tethered, so that it can only rotate around a vertical axis, and rotations are computed as yaw angles, see figure 3.1. A narrow vertical bar - which is going to be called the external input - is going to be displayed on the dark screen, and made travel around the arena. In this experiment the activity in the fly's EB is measured, and evidence shows that the bump of activity in the brain follows the external input while the fly rotates in the arena.

Aim of this work is to reproduce the experiment mathematically in such a way that the “*in silico*” model (the simulation) behaves such as the fly does in the real world experiment. It has been shown that the EB can be divided into 16 domains, called wedges, each of which containing synapses of the E-PG neurons, and that neurons in each wedge have the same preferred firing direction, thus each wedge covers a range of directions of 27.5° . We decided to model the EB as a neural field, because we are interested in the display of activity throughout the EB. Since the EB has a toroidal structure - but dividing it into wedges we are only interested in the angular position of each one - we can make a simplification considering the EB as a ring. The structure of the EB network of neurons allows us to model it as a ring attractor [6, 9, 12, 16, 20, 24].

Neural fields are easily studied in their continuum limit, as was presented in the previous section. However, since we are dealing with a ring that needs to be discretized into 16 sections we wish to write the model in its discretized version. The first section of this chapter, 3.1, contains the description of the discretized model, while in section 3.2 results are presented, and it is shown that our model - with a certain choice of parameters - reproduces the fly’s behavior, as expected. Lastly, in section 3.3 we study the case in which the input is abruptly moved away of a certain angle in the LED arena, and see if the modelled bump of activity jumps as well. We are showing that this happens depending on the strength and width of the input and also on the width of the jumping angle, so a bifurcation analysis is going to be performed.

3.1 Discretization of neural field

Once we simplify the structure of the EB into a ring, we also represent the ring as a periodic interval, so any position on the ring is described by an angle $\theta \in \Omega$, where $\Omega = (-\pi, \pi]$ is a periodic domain. The discretization Θ of Ω is made by defining $\Delta\theta = 2\pi/n$, where $n = 16$, and $\Theta = \{\theta_i = -\pi + i\Delta\theta\}_i$, $i = 1, \dots, n+1$. Note that θ_1 and θ_{n+1} coincide.

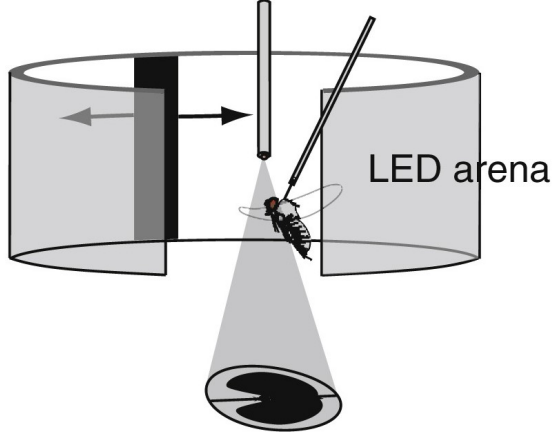


Figure 3.1: A tethered fly in a LED arena with the vertical input bar rotating around the screen and the fly rotation around its vertical axis. Picture adapted from [11].

A discrete version of the neural field on this domain is:

$$U'(t) = -U(t) + Mf(U(t)) + I(t) \quad (3.1)$$

where U is a vector encoding the activity on the ring Ω . In order to study the dynamics of this equation we are going to borrow theory from continuous neural fields, which we extensively described in the previous chapter. Below, there is a brief construction of this equation.

In equation 3.1 U is the activity on Ω , and is a vector of $n + 1$ components, where $n = 16$ and the first and last components are set to be equal, to encode periodicity. To make a connection with continuous neural fields, $U_i(t) = u(\theta_i, t)$ and $U'_i(t) = \partial_t u(\theta_i, t)$. The matrix M is the connectivity matrix and is defined as

$$M_{ij} = W(\theta_i - \theta_j)\Delta\theta$$

where $W(z)$ is the connectivity function, as defined in the previous chapter. Here we are choosing

$$W(z) = a_1 \exp(-b_1|z|) - a_2 \exp(-b_2|z|)$$

Each element M_{ij} of matrix M represents the connectivity between neurons at position θ_i and neurons at position θ_j .

In order to make computations, $W(z)$ is periodically extended in the MATLAB code. Again, a positive value of $W(z)$ means that there is an excitatory connection between neurons, while a negative value indicates inhibition. The choice of parameters a_1, a_2, b_1, b_2 influences how strong excitation and inhibition is between neurons.

The function $f(U)$ is the firing rate function and is chosen to be a sigmoid:

$$f(U) = \frac{1}{1 + \exp(-\mu(U - h))}.$$

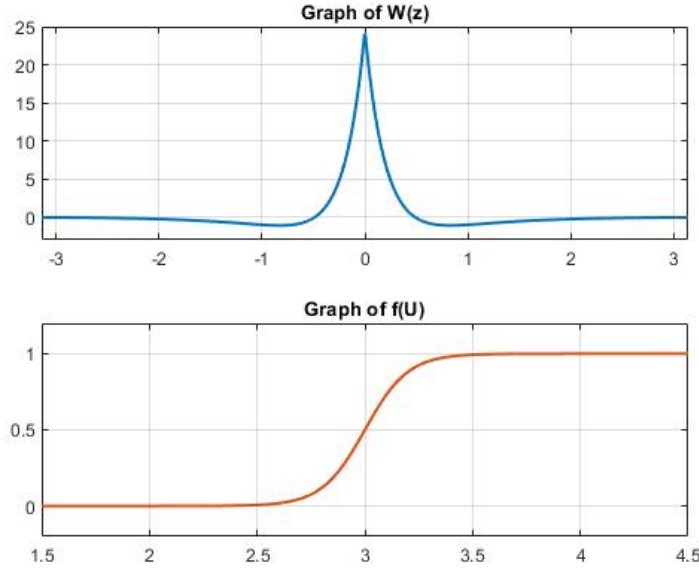


Figure 3.2: Graphs of $W(z) = a_1 \exp(-b_1|z|) - a_2 \exp(-b_2|z|)$ and $f(U) = \frac{1}{1+\exp(-\mu(U-h))}$, with set of parameters $\mu = 10$; $h = 3$; $a_1 = 30$; $b_1 = 5$; $a_2 = 5.5$; $b_2 = 1.5$.

A graph of $W(z)$ and $f(U)$ can be found in figure 3.2.

Lastly, $I(\theta, t)$ is the input at time t and position θ . Since we want to sum vectors, we need to transform the continuous input into a vector. Thus we evaluate it at $\Theta = \{\theta_i\}_i$, $i = 1, \dots, n + 1$, calling $I(t) := I(\Theta, t)$ the vector of $n + 1$ components, where first and last components are equal for periodicity.

3.2 Results of simulations

When no input ($I(t) \equiv 0$) is applied to the system - corresponding to a “resting” condition on the fly - a bump of activity arises (and is stable for a certain set of parameters). The position of this bump can be influenced by changing initial conditions. Thus, by choosing as initial condition a function centered at 0,

$$U_0(\theta) = 0.5(\cos(\theta) + 1)^3$$

the bump arises at $\theta = 0$, as seen in figure 3.4a. It is interesting to notice that the bump is sustained for the whole time of the simulation. With a translation of the initial condition, namely centering it at $\theta = -1.5$ instead of 0,

$$U_0(\theta) = 0.5(\cos(\theta + 1.5) + 1)^3,$$

we notice that a bump arises as well, and is centered at $\theta = -1.5$. See figure 3.4b. This was expected and is due to the rotation invariance of the system explained in section 2.3.

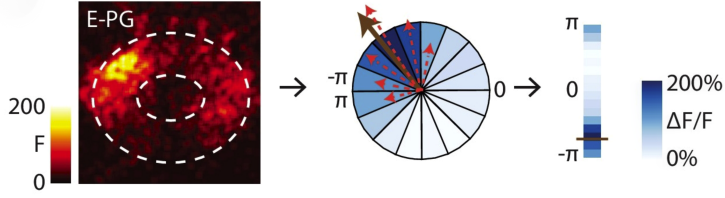


Figure 3.3: A bump in HD cells (left) registered with a two-photon imaging technique, and a graphical representation of the activity bump on the ring (right). Darker colors represent higher activity. Dashed arrows are averaged to compute the PVA, represented by the black arrow in the ring and the red line in the interval $(-\pi, \pi]$. Picture adapted from [22].

What we see when the fly is “at rest” is the same result as when the fly is moving in darkness. In fact, in biological experiments, even when the scenery is moving (or the fly is moving around within this scenery) but no input is applied, the bump remains still during the whole time of the experiment. In that case the fly uses sensory stimuli other than the visual ones in order to orientate in space [6].

It is interesting to notice that even if applying an initial condition with small magnitude, the bump arises anyway and sets to a certain value. This meaning that the bump is a basin of attraction for the system, so any localized perturbation of the zero equilibrium is attracted by the bump equilibrium. In figures 3.4c and 3.4d we represented the initial condition in blue, and the bump at the end of the simulation $t = 20$ in red. The initial condition is way smaller (and also wider) than the final aspect of the bump.

Consider now the case when the fly is moving and the environment is not dark: this situation is replicated in the arena by turning on a vertical bar in the LED arena, and make it rotate on both directions. The animal starts following this input rotating around its fixed spot, and thus the activity bump should follow the input as well, even with some systemic delay. In order to replicate this experiment we defined different possible stimuli, and applied them to the system with equation 3.1. The head direction of the fly is measured using the PVA, Population Vector Average, figure 3.3. PVA is an averaging of the activity over all the possible positions in the fly’s head, the 16 wedges defined above. The angle of PVA is then used as direction of the fly’s head.

With the first input applied, we are checking what happens to our modelled fly when the velocity of the input changes rapidly. Results can be seen in figure 3.5. The bump follows the input for the whole simulation, varying its velocity as the input

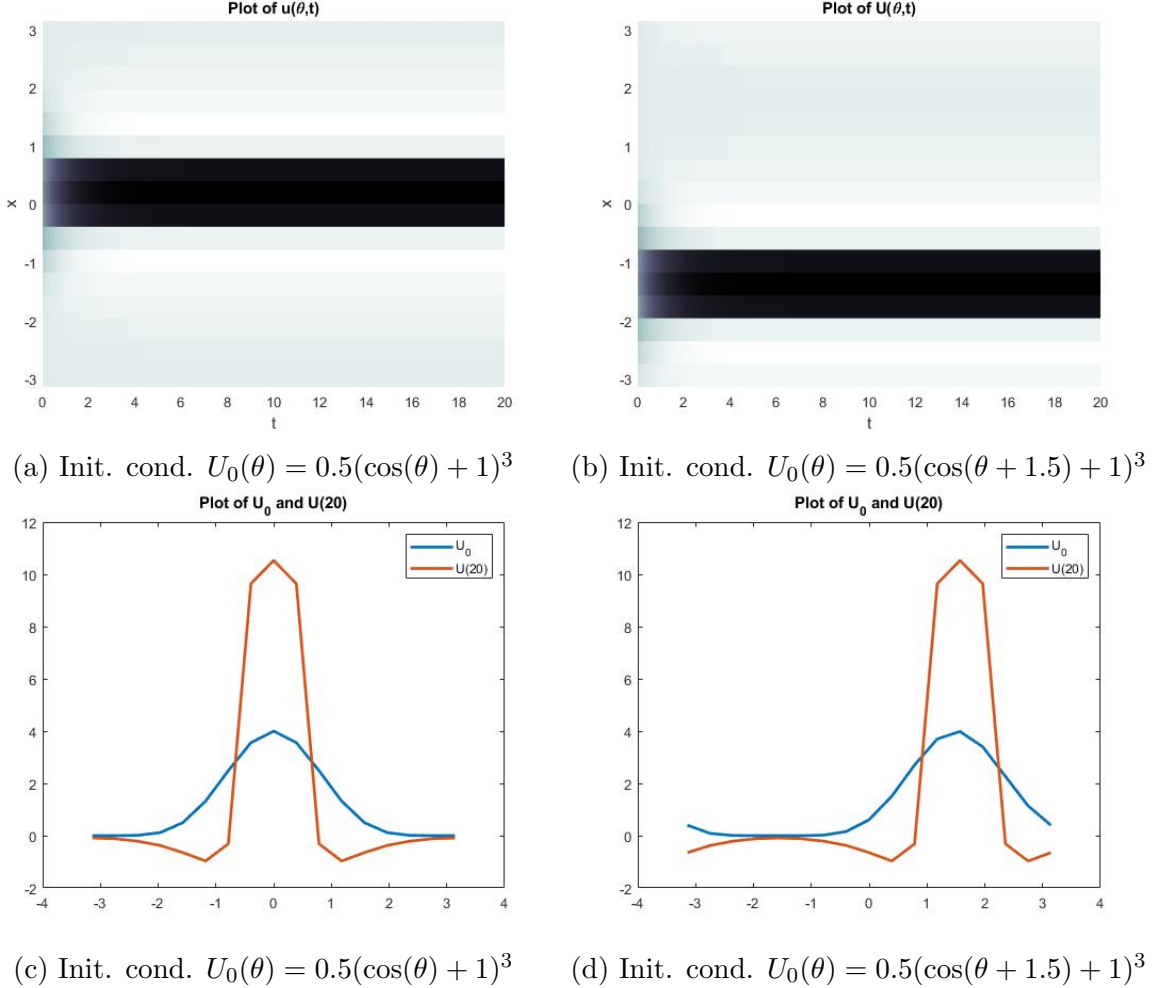


Figure 3.4: Visualization of the bump at rest. Choice of parameters: $\mu = 10$; $h = 3$; $a1 = 30$; $b1 = 5$; $a2 = 5.5$; $b2 = 1.5$. In figure (a) the bump is centered at $\theta = 0$, while in figure (b) at $\theta = -1.5$, because of different initial conditions. (c) and (d). Blue line is the initial condition, and red line is the bump at the end of the simulation $t = 20$. In both cases it is visible that the bump arises even with a very small initial condition, thus the bump equilibrium is a basin of attraction for the model.

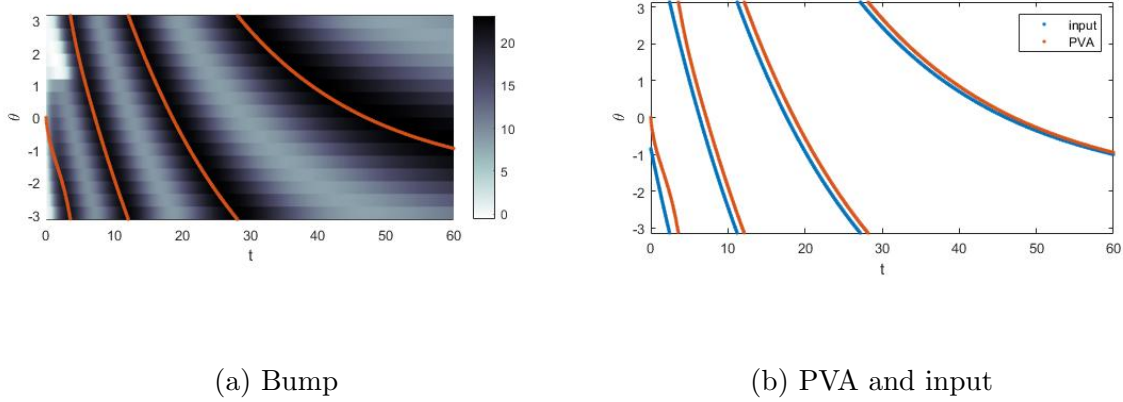


Figure 3.5: Visualization of the bump with input with varying velocity. $I(\theta, t) = 15(\cos(\theta/2 - c(t) + 1))^2$, where $c(t) = 10 \exp(-t/20)$. Initial condition $U_0(t) = 0.5(\cos(\theta) + 1)^3$. Choice of parameters: $\mu = 10$; $h = 3$; $a_1 = 30$; $b_1 = 5$; $a_2 = 5.5$; $b_2 = 1.5$. Red line represent the head direction of the fly in the visual arena measured as PVA, while blue is the position of the vertical bar (the external input). It can be seen that the fly starts following the input bar in the arena, as the PVA of activity in EB follows the external input.

does. When the input decreases its velocity towards the end of the simulation $t \approx 50$, the PVA is closer to the input, meaning that the systemic delay is progressively reduced. This was expected, because it is easier for the fly to follow a stimulus at lower velocities.

With an oscillating input, instead, applied for a smaller interval of integration, $[0, 20]$, it can be noticed that the bump follows the input, even if most of the peaks of $I(t)$ get smoothed by the discretization of the system. This means that inputs changing too rapidly are not recognised by the fly, which can follow only slower oscillating inputs.

3.3 Input jumps and bifurcation analysis

It is interesting to study what happens to the bump when an external input is suddenly moved to a different position in the visual arena. An oscillating input is applied and travels the led arena for a specific amount of time, after which it is moved of a certain angle, resulting in a “jump”. In most cases the bump, that was already following the external input, follows the jump as well, with a systemic delay, as expected. It is thus possible to exert a forcing on the bump of activity position by just moving the input abruptly. In other cases, instead, the bump adjusts its position without abrupt changes, a phenomenon that we are going to call “flow”. The bump jumps depend on several parameters: strength and width of the input and also the angle of jumps. By input strength we mean the maximum value of the input $I(t)$ and since it is chosen as a

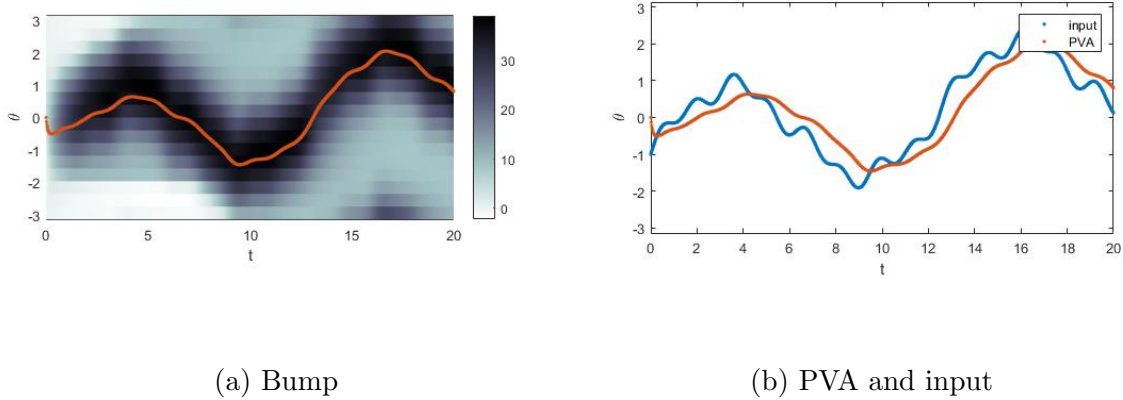


Figure 3.6: Visualization of the bump with oscillating input $I(x, t) = 8(\cos(x - c(t)) + 1)^2$, where $c(t) = -1 + 0.2 \sin(4t) + 0.2 \sin(2t) + 1.5 \sin(0.5t) + 20 \sin(0.005t)$. Initial condition $U_0(t) = 0.5(\cos(\theta) + 1)^3$. Choice of parameters: $\mu = 10$; $h = 3$; $a_1 = 30$; $b_1 = 5$; $a_2 = 5.5$; $b_2 = 1.5$. Red line represent the head direction of the fly in the visual arena, while blue is the position of the vertical bar (the external input). It can be noticed that the fly follows the external input, with a smoothing effect, as the discretization of the EB is too coarse to follow variations with high frequency.

bump as well, the width is measured as Δ in section 2.3. In figure 3.7 we show results when a jump of 150° is applied to the input $I(\theta, t) = 8(\cos(\theta - c(t)) + 1)^2$ with velocity $c(t) = -1 + 0.2 \sin(4t) + 0.2 \sin(2t) + 1.5 \sin(0.5t) + 20 \sin(0.005t)$.

In this figure we present another measure of the fly's position, in addition to PVA. It's easily noticeable that the PVA changes very slightly, even when the jump is applied at $t \approx 15$. The bump, instead, moves very rapidly, see figure 3.7a. Since we wish to construct a bifurcation diagram for jumps, depending on strength and width of the input, we need a "measure" for jumps that distinguishes the cases when there is a jump and when there is a flow. The second measure we choose is defined as the maximum of $U(t)$ over all its components and is depicted in figure 3.7 in green.

In addition to jump and flow outcomes, a third case is possible: when the input is not strong enough to move the bump from its resting position. This one will be referred to as "no effect". Thus in order to distinguish between the three outcomes we defined a criterion, for which we compute the maximum absolute difference between any two points of $U(t)$ computed over all the time instants of the simulation, then outcomes are associated as follows:

- If the difference is 0, no effect,
- if the difference is between $\Delta\theta$ and $2\Delta\theta$, flow,
- if the difference is bigger than $2\Delta\theta$, jump.

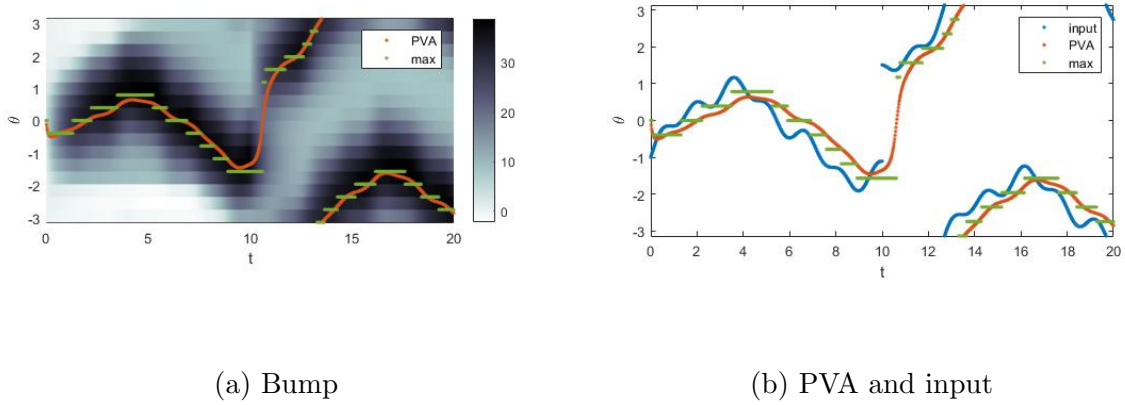


Figure 3.7: Visualization of the bump with input $I(\theta, t) = 8(\cos(\theta - c(t)) + 1)^2$, where $c(t) = -1 + 0.2 \sin(4t) + 0.2 \sin(2t) + 1.5 \sin(0.5t) + 20 \sin(0.005t)$. The input jumps of 150° at time Initial condition is given as $u_0(\theta) = 0.5(\cos(\theta) + 1)^3$ Choice of parameters: $\mu = 10$; $h = 3$; $a1 = 30$; $b1 = 5$; $a2 = 5.5$; $b2 = 1.5$. Red line represent the head direction of the fly in the visual arena, while blue is the position of the vertical bar (the external input). It can be noticed that the fly follows the external input. The jump in the bump of activity is more visible in figure (a) than with the PVA.

Since with this choice of input, a travelling wave of the form $s(\cos\theta + 1)^p$, the strength depends both on the exponent p and the constant s , in the code the input is going to be normalized, in such a way that the strength is defined by the constant s :

$$\tilde{I}(\theta, t) = s \frac{I(\theta, t)}{\max_{\theta}(I(\theta, 0))}.$$

Then for four choices of jump angles - 60° , 90° , 120° and 150° - a bifurcation diagram is produced, with the above criterion, and by varying the strength and width parameters. They are shown in figure 3.8. For low values of the angle, the “flow” area is bigger, and it reduces with increasing angles. Also, we notice that the flows arise for big values of the input width and they depend on the input strength only for high angles (120° and 150° , see figures 3.8c and 3.8d). This means that when the input is too wide the HD cells in the fly’s EB are not able to detect abrupt differences in the input position. The same happens for small angles.

With these experiments we concluded that the model is able to reproduce the fly’s behavior in the visual arena experiments. Some further analysis is still possible, though. For example, it would be interesting to study how fast the input can oscillate in order for changes to be recognised by the fly’s brain, since the discretization of the EB inevitably produce a smoothing effect on applied inputs.

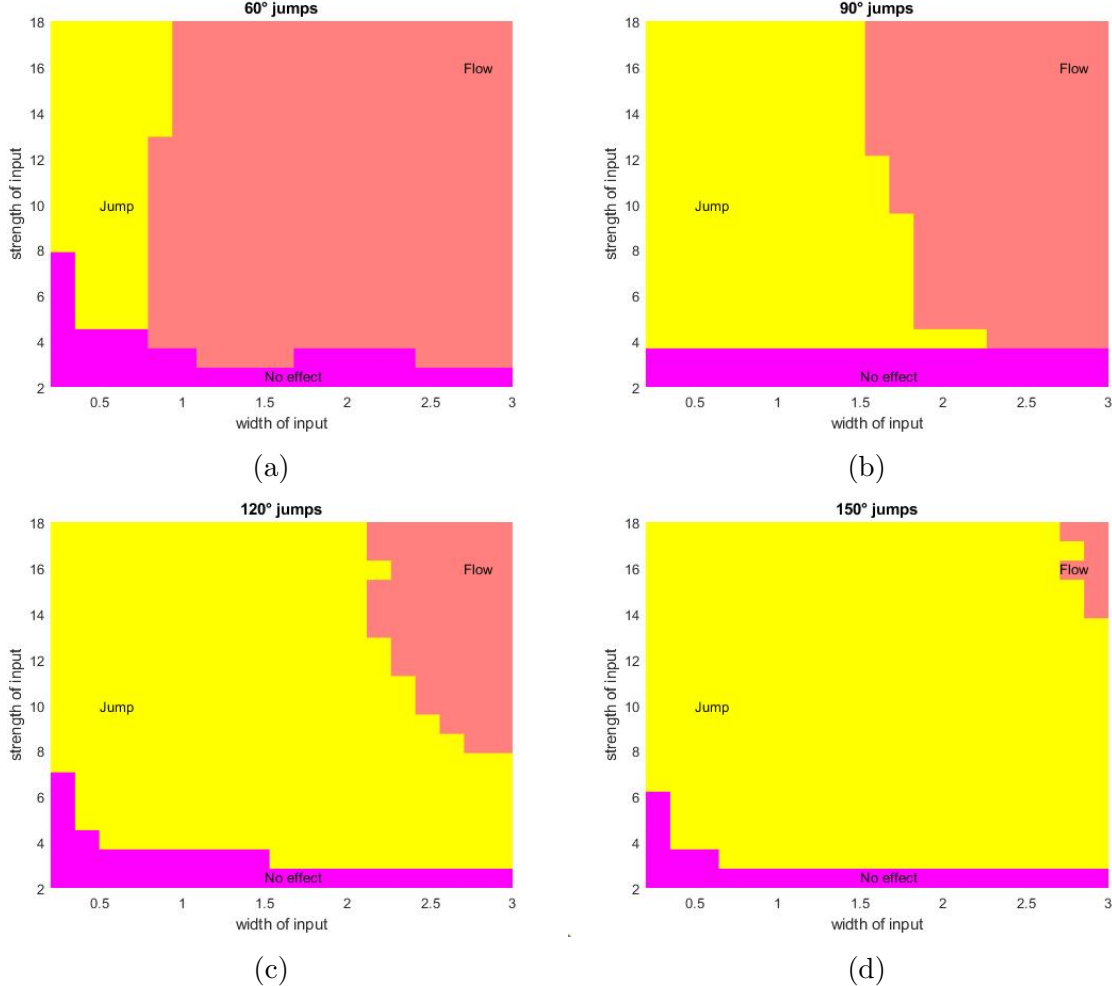


Figure 3.8: Bifurcation diagrams for several values of the input jump angles, with varying strength and width of the input. The yellow area represents “jumps”, the pink area “flows” and the purple one “no effect” of the input on the jumps. The flow area arises for big values of the width and possibly high values of the strength (c) and (d). It slowly reduces with increasing jump angles, meaning that the bigger the jumps are the more they are recognised by HD cells in the fly’s EB.

4 Path integration

In addition to the heading mechanism discussed and modelled in the previous chapter, *Drosophila* [14] and other insects - such as bees [17], cockroaches [8] and locust [5] - are able to perform path integration a simplified version with respect to mammals. This is made possible by the information encoded in CX neurons, and by the specific connectivity of CX neuropils.

In fact, it has been shown that P-EN neurons are connected to E-PG neurons and thus are able to store memory about the movements performed by the insect, allowing a straight-line return to its initial position [17, 18]. A biological structure of the network and the functions can be found in section 4.1. Then we describe the network mathematically in section 4.2 and propose results in 4.3.

In our work, we are considering a tethered fly, so we are interested in its capability of returning to its initial direction. However, it is easily possible to apply modifications to our model in order to study a fly moving in a 2-dimensional space.

4.1 Description of the biological network

Stone et al. [17] propose an organization in the CX as follows. A first population of neurons, called TB1 population, residing in the PB, receives direct input from cells in the EB [14]. Since cells in the EB are HD cells, and each of them represents a specific head direction (through their preferred firing directions), then each of the TB1 neurons behaves in the same way. TB1 neurons are two populations (one left and one right) of eight neurons encoding the head direction, see figure 4.1, thus for each of the eight possible preferred directions (distanced from each other by an angle of 45°) there are two PB neurons. Since they are identical, with identical behavior and identical connections with other populations, we are going to consider each of these couples as a single cell.

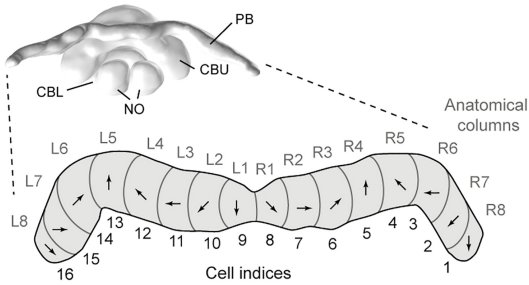


Figure 4.1: TB1 neurons in the PB. Arrows in each glomerulus represent the preferred direction of TB1 neurons residing there. Note that the same preferred direction is held by two glomeruli, one in the left and the other in the right areas of the PB Picture adapted from [17]

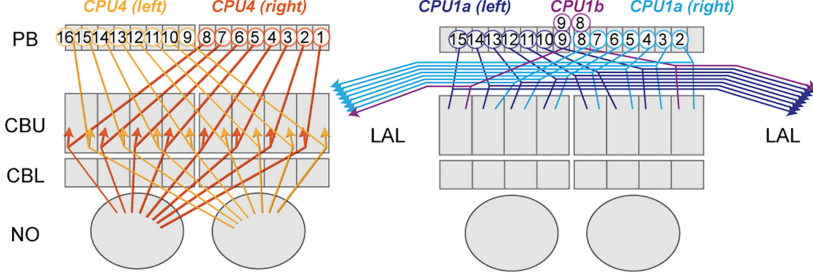


Figure 4.2: CPU4 and CPU1 neurons in the PB. Note that they follow two different projection patterns, in fact they occupy different glomeruli in the PB. Picture adapted from [17]

TB1 cells are inhibitory towards themselves and other two populations, CPU1 and CPU4, that we are going to refer as the “steering” and “memory” populations respectively. TB1 cells compose a local excitatory and distal inhibitory network, creating a ring attractor connectivity structure [24]. In particular, the local excitation is only a self-excitation, while the inhibition acts on all other population cells, with inhibition strength growing along distance. Additionally, each TB1 cell inhibits two pairs of cells, one from CPU1 and the other from CPU4 populations. Both these populations reside in the PB as well, following different projection patterns [17]. In fact, they occupy shifted positions in the glomeruli, as can be seen in figure 4.2, for a total of 18 glomeruli.

CPU4 population is referred to as “memory” population because these neurons encode information about which head directions cells have been activated during the route, thanks to the connection with TB1 neurons. They also receive an excitatory input, this time from another population, TN, residing in the noduli. Each of the two noduli (left or right) gets activated when the animal is rotating counterclockwise or clockwise respectively. TN neurons excite all the left or right CPU4 populations simultaneously depending on the direction of the rotation, allowing the CPU4 population to store information on how much the animal rotated in each direction. In a 2D setting, TN also encode information relative to the speed at which the animal is moving while rotating in one or the other sense.

Finally, CPU1 neurons receive inhibitory input from TB1 neurons, and excitatory input from CPU4 cells. They compare the current and desired direction in order to produce a steering signal [17]. A schematic representation of global connections in the CX can be found in figure 4.3, while connections of single neurons can be found in figure 4.4. The right CPU1 population receives input from the left CPU4 population and vice versa. This reflects in the kind of information encoded in CPU1 neurons. In particular, we are not interested in the activity level of single neurons in this population. Instead, what is meaningful is the difference in the cumulative activity in right and left populations. In fact, this quantity represents the amount of steering needed by the animal in order to retrieve its initial position. Even if the fly has been oscillating around its fixed axis, what is important is the cumulative difference between how much it has

moved in one and the other direction.

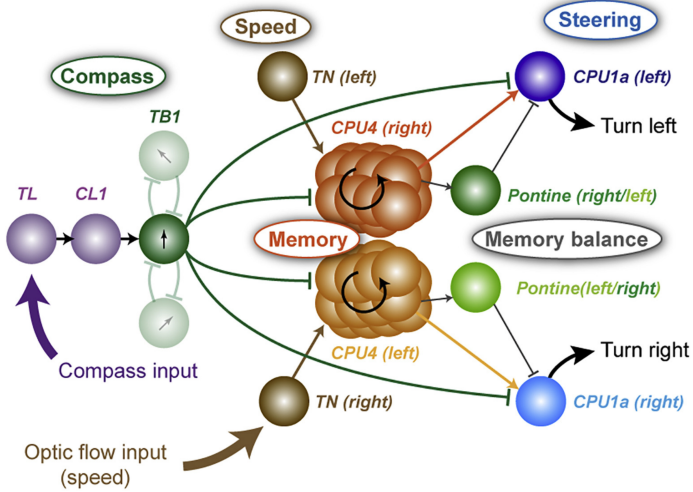


Figure 4.3: Schematic representation of global connectivity in the PB. Picture adapted from [17]

Thus, during the fly's journey, TB1 cells generate a bump of activity, signaling the instantaneous head direction of the animal. This information is then stored in the memory cells (CPU4), together with speed and direction of rotation, in order to keep a cumulative track of how much the fly has moved in each direction. Then information about memory is processed in steering cells (CPU1), in order for the fly to be able to retrieve the initial position. In particular, our experiment consists in letting a tethered fly move in the arena following a visual stimulus, suddenly removing this stimulus, and checking if the fly is able to turn back to where it started. Instead of following the outbound route back to the initial position, repeating all the oscillations, the fly rotates back in a unique direction dictated by steering cells, until the position is reached and the steering signal from CPU1 cells stops. In a 2D setting the animal is able to return to the initial position with a mechanism similar to the one in 1D, integrating information about velocity as well. In this case the home-returning path is performed in a straight-line fashion.

4.2 Mathematical modelling of the network

TB1 population could be modelled as a discretized neural field with 8 sectors, choosing sigmoid firing rate function and connectivity function such that there only is self-excitation, while inhibition is increasing along distance. Using results from the previous experiment, we model the activity in TB1 population with a neural field, with input a travelling wave. The input is then defined as:

$$I(t) = (\cos(\Theta - \theta(t)) + 1)^5$$

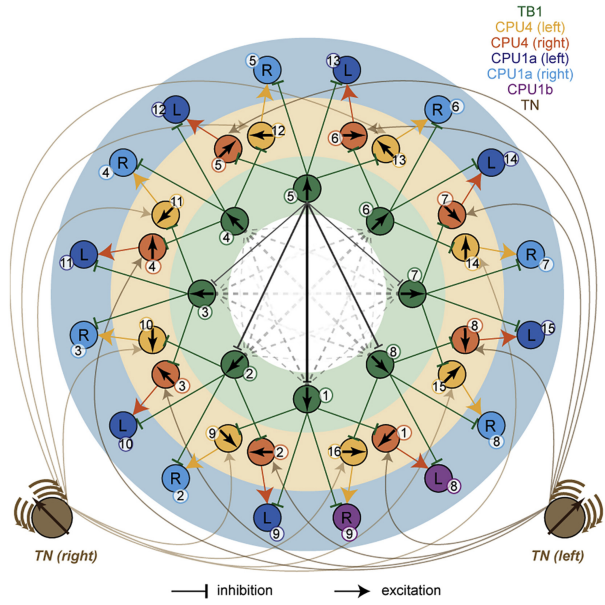


Figure 4.4: Schematic representation of connectivity among neurons in the PB. Width of the arrows represent strength of the connections between neurons. Picture adapted from [17]

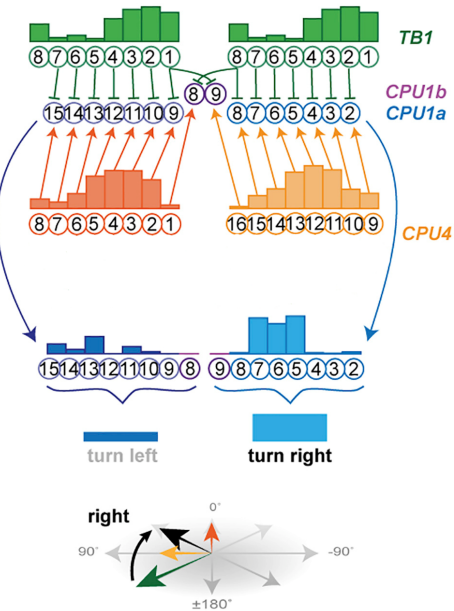


Figure 4.5: Activity of the three populations of neurons. The arrows in the last row represent the PVA for corresponding populations. Steering is positive, so to restore initial position (black arrow) the fly must turn right. Picture adapted from [17]

where Θ is a discretization of the interval $\Omega = [-\pi, \pi]$ in $n + 1$ points, with $n = 8$ and the input position $\theta(t)$ is the solution to the ODE:

$$\dot{\theta}(t) = S_i(t)$$

with $S(t)$ an assigned function, encoding the velocity of stimuli, be it the external input in the first part of the experiment, and - once removed - the internal steering input.

So, defining the activity of the first population as $U(t)$, where U is a vector of $n + 1$ components, the equation becomes:

$$\dot{U}(t) = -U(t) + M_1 f(U(t)) + I(t)$$

Such as in chapter 3, matrix M_1 is constructed from a mexican hat function.

$$(M_1)_{ij} = W(\theta_i - \theta_j)$$

where $W = a \exp(-|z|) - c$, with appropriate parameters a and c .

The inhibition from TB1 population to CPU4 population is easily implemented by subtracting the activity U in the model equation of CPU4 population, whose activity is going to be indicated as $Z(t)$. In order to model excitation coming from the noduli, we are going to make an assumption: we are not considering the noduli as populations of neurons. Instead, since the right and left CPU4 populations only receive input if the animal is rotating clockwise or counterclockwise respectively, and since the rotation is given by the sign of the stimulus speed $S(Z_R, Z_L, U, t)$ and affects all CPU4 neurons of one populations identically, we are going to use positive and negative parts (respectively) of $S(t)$ as excitatory inputs. Recall that if $S(Z_R, Z_L, U, t)$ is positive, the fly is moving to the right, and vice versa if it is negative. Positive and negative parts are defined, for any function $F(t)$ as

$$F_+(t) = \max\{F(t), 0\} \quad \text{and} \quad F_-(t) = \max\{-F(t), 0\}$$

The functions S_+ and S_- are going to be multiplied by a constant α in order to modulate the magnitude of the excitatory input. In the same way, the magnitude of inhibitory input is going to be modulated by multiplying $U(t)$ by a parameter β .

In addition, every CPU4 neuron has a self-excitatory component. This could be modelled by using a neural field, but the connectivity function would be positive only in 0 and null otherwise, making the self-excitation equal to the term $M_2 f(Z)$, where M_2 is an identity matrix multiplied by a constant and $f(Z)$ is the usual sigmoid function. Lastly, memory decay needs to be taken into consideration, and thus we introduce a memory decay constant m and we multiply it times the activity level of population Z .

Calling $Z_R(t)$ and $Z_L(t)$ the vector fields representing activity of respectively right and left CPU4 neurons at time t , we can write the evolutionary equations for the “memory” population:

$$\begin{cases} \dot{Z}_R = -mZ_R + \alpha S_+(Z_R, Z_L, U, t) - \beta U + M_2 f(Z_R) \\ \dot{Z}_L = -mZ_L + \alpha S_-(Z_R, Z_L, U, t) - \beta U + M_2 f(Z_L) \end{cases}$$

It is convenient to divide also CPU1 neurons into left and right populations, that we are calling $V_R(t)$ and $V_L(t)$. Each of these neurons receives an inhibitory input from a neuron of the TB1 population and an excitatory one from a CPU4 neuron from the opposite side (V_L receives excitation from Z_R and V_R from Z_L), so CPU1 populations's activity can be described using the mapping

$$(Z, U) \mapsto Z - U$$

that for the left and right populations becomes:

$$\begin{cases} V_L(Z_R, U) = Z_R - U \\ V_R(Z_L, U) = Z_L - U \end{cases}$$

The exact connections between neurons and the shifting between TB1 and CPU1 populations (see figure 4.5) are going to be implemented precisely in the MATLAB code, by using the function “circshift”.

As said above, the single levels of activity in CPU1 are not as interesting as the population as a whole. Thus we define a quantity, namely the “steering”, being the difference between integral of right and left populations. In fact, if this quantity is positive, the fly needs to turn to the right (clockwise) in order to retrieve the initial position. Vice versa if negative. Steering is defined as

$$G(Z_R, Z_L, U) = \sum_{i=1}^8 V_R(Z_{L,i}, U_{i+1}) - \sum_{i=1}^8 V_L(Z_{R,i}, U_{i-1})$$

Once we remove the external stimulus, the new speed of the travelling wave needs to be made dependent on the steering quantity. In order to do so, we define a new speed as

$$S_2(Z_R, Z_L, U) = \tanh(G(Z_R, Z_L, U)/\tau)$$

We choose tanh as it is bounded between -1 and 1, and conserves the sign of G . In fact, as we said, if the steering is positive we want the fly to be moving to the right (clockwise), and to the left if it is negative, so we want respectively a positive or negative input velocity.

Using all the information gathered until now, we can define our full model as a dynamical system

$$\begin{cases} \dot{U} = -U + M_1 f(U) + I(t) \\ \dot{Z}_R = -mZ_R + \alpha S_+ - \beta U + M_2 f(Z_R) \\ \dot{Z}_L = -mZ_L + \alpha S_- - \beta U + M_2 f(Z_L) \end{cases} \quad (4.1)$$

The angular velocity of the fly, $S(Z_R, Z_L, U, t)$ is defined as

$$\begin{cases} S(Z_R, Z_L, U, t) = S_1(t) & \text{for } t < T \\ S(Z_R, Z_L, U, t) = S_2(Z_R, Z_L, U) & \text{otherwise} \end{cases}$$

where S_1 is the velocity of the external input, and is assigned, while S_2 is the returning velocity, given by internally available information, and $t = T$ is the instant when the external stimulus $I(t)$ is removed.

4.3 Results of input application

Initially, for simplicity we choose a constant velocity, $S_1 = 1.26$, and deciding to let the fly move of only π radians, we apply this input for 1.66 seconds. The fly's journey can be seen in figure 4.6a, where at time $t = 1.66$ the input is released and the fly starts following a new input with velocity $S_2(t)$ (as defined above), until the steering G is null, and up to its final position.

In this experiment, the internal input at time $t = 1.66$ is negative. In fact, as seen in figure 4.6c, the activity of left CPU1 is way higher than activity of right CPU1 and $G(1.66) = -428.2$. It is interesting to notice that once it reached this position, namely at time $t \approx 6$, the fly is able to stay there without moving anymore, because no new input is applied. In fact $G(6) = -4.4$, being very close to 0. It is interesting to notice that from figure 4.6c to 4.6d all the populations decrease. This is due to the memory decay. In fact, by choosing a smaller constant m one can obtain populations that do not decrease this much in time, and then memory can be stored for longer periods.

Then, with the same choice of parameters, an input with oscillating velocity was chosen and applied for 7 seconds. As can be seen in figure 4.7a, at time $t = 7$, when the external input is suddenly removed, the fly inverts its direction of motion and starts returning back, moving counterclockwise. In fact $G(7) = -405.9$, and similarly to the previous case, it stays at position $\theta = 0$ once it is reached again, because $G(12) \approx 10^{-6}$. A visualization of activity of CPU1 and CPU4 neurons as bar charts at time $t = 7$ is visible in figure 4.7c. Here level of V_L is again cumulatively bigger than level of V_R .

This choice of parameters allowed the fly to return to its initial position. However, this is not always the case: the fly is always able to "return" in the correct direction, but it often travels more or less than needed, see for example figure 4.8. There, we applied another oscillatory stimulus for 7 seconds and when we removed it, the fly started turning back, with some delay. Steering at time $t = 7$ was positive, $G(7) = 402.6$, because cumulative activity of V_R was bigger than V_L and thus the fly started turning right. However, in this case it stopped before reaching the exact initial position ($\theta = 0$).

This phenomenon is due to two factors: the memory decay and the self-excitation of CPU4 populations. In fact, they both depend on the activity of the population itself ($Z_L(t)$ and $Z_R(t)$), see equation 4.1, and so for higher activity there is higher memory decay and self-excitation. This means that the more one of the populations is active, the bigger the effect of memory decay and self-excitation is. In order to have different outcomes to this experiments, thus, one needs to change and tune parameters m and M_2 .

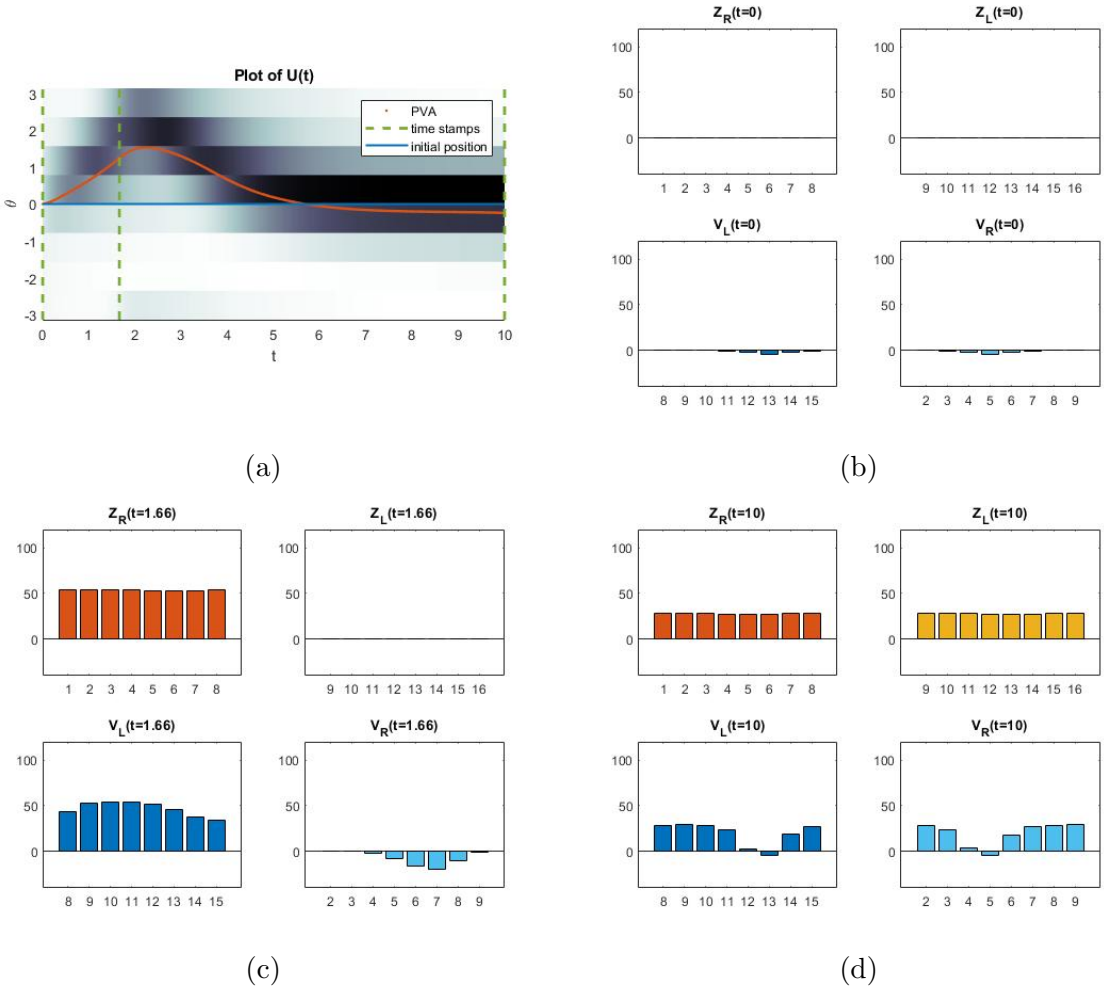


Figure 4.6: (a). Activity of $U(t)$ with choice of parameters: $m = 0.1$; $\alpha = 20$; $\beta = 0.01$; $M_2 = 10$; $\mu = 10$; $h = 1$; $a = 2$; $c = 0.5$; $\tau = 100$ and constant input $S_1(t) = 1.26$ applied for 1.66 seconds. The red line represents the fly's HD, computed as PVA. When stimulus is removed at $t = 1.66$, the fly starts rotating back to initial position (blue line) that is maintained once it is reached.

(b), (c), (d). Bar plots: visualization of CPU4, first row, and CPU1, second row of each figure at different moments in time. Each bar represents activity of corresponding glomerulus. At time $t = 0$ there has been no rotation, so both Z_L and Z_R are null. V_L and V_R are negative because only U affects them negatively. When stimulus is removed, $t = 1.66$ the steering is negative $G(1.66) = -428.2$ and makes the fly turn left until it becomes close to 0, maintaining the final position for the rest of the simulation, $G(10) = -0.002$. Populations decreasing from (c) to (d) is an effect of memory decay.

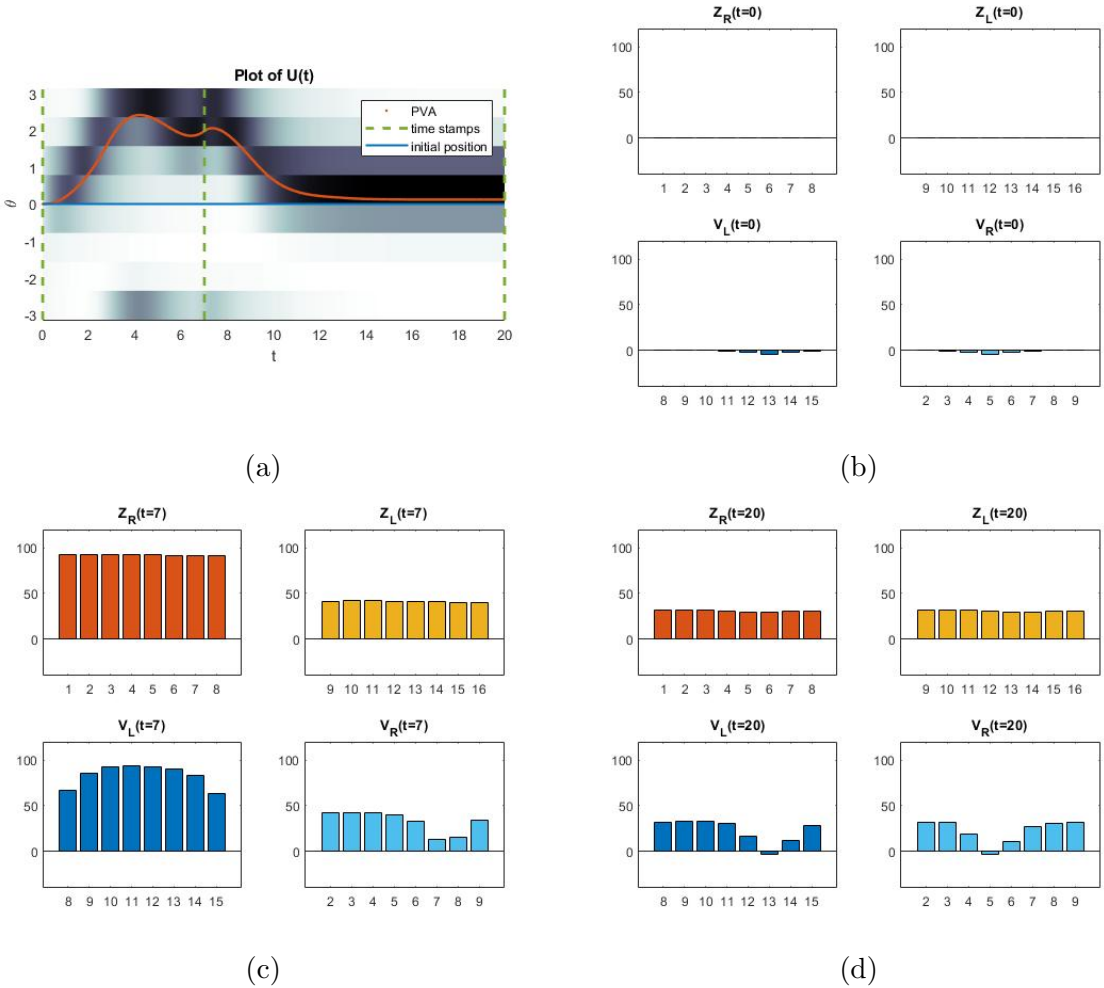


Figure 4.7: (a). Activity of $U(t)$ with choice of parameters: $m = 0.1$; $\alpha = 20$; $\beta = 0.01$; $M_2 = 10$; $\mu = 10$; $h = 1$; $a = 2$; $c = 0.5$; $\tau = 100$ and input with oscillating velocity $S_1(t) = \sin(t) + 0.5 \sin(0.2t)$ applied for 7 seconds. The red line represents the fly's HD, computed as PVA. When stimulus is removed $t = 7$, the fly starts rotating back to initial position that is maintained once it is reached, see the blue line.

(b), (c), (d). Bar plots: visualization of CPU4, first row, and CPU1, second row of each figure at different moments in time. Each bar represents activity of corresponding glomerulus. At time $t = 0$ there has been no rotation, so both Z_L and Z_R are null. V_L and V_R are negative because only U affects them negatively. When stimulus is removed, $t = 7$, the steering is negative $G(7) = -405.9$ and makes the fly turn left until it becomes close to 0, maintaining the final position for the rest of the simulation, $G(20) \approx -10^{-6}$. Populations decreasing from (c) to (d) is an effect of memory decay.

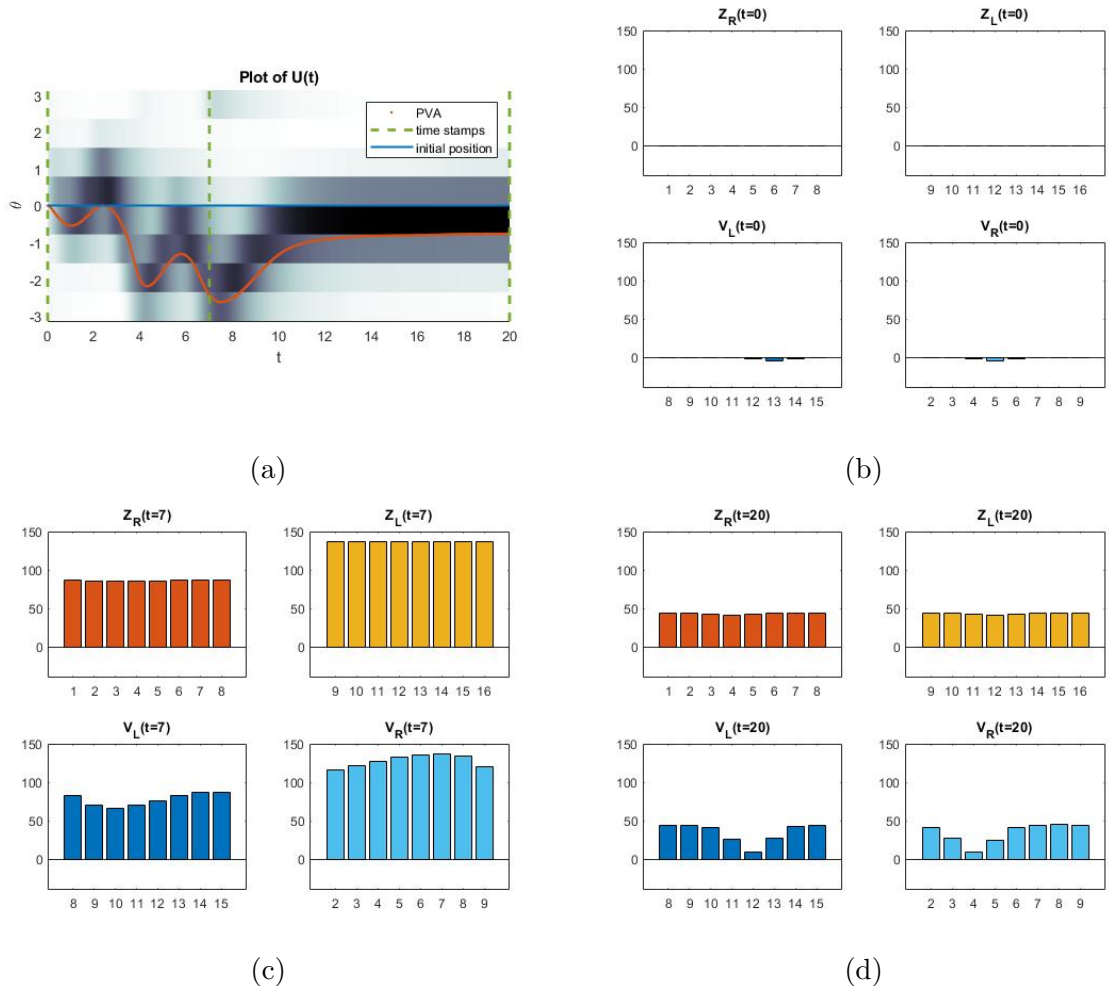


Figure 4.8: (a). Activity of $U(t)$ with choice of parameters: $m = 0.1$; $\alpha = 20$; $\beta = 0.01$; $M_2 = 10$; $\mu = 10$; $h = 1$; $a = 2$; $c = 0.5$; $\tau = 100$ and input with oscillating velocity $S_1(t) = 0.3 \sin(t - 10) + 0.4 \sin(0.2(t - 10)) + 2 \sin(2(t - 10))$ applied for 7 seconds. The red line represents the fly's HD, computed as PVA. When stimulus is removed $t = 7$, the fly starts rotating - with some delay – back towards its initial position (blue line) that is not reached in this case, even if the final position is maintained once it is reached.

(b), (c), (d). Bar plots: visualization of CPU4, first row, and CPU1, second row of each figure at different moments in time. Each bar represents activity of corresponding glomerulus. At time $t = 0$ there has been no rotation, so both Z_L and Z_R are null. V_L and V_R are negative because only U affects them negatively. When stimulus is removed, $t = 7$, the steering is negative $G(7) = 402.6$ and makes the fly turn left until it becomes close to 0, maintaining the final position for the rest of the simulation, $G(20) \approx 10^{-6}$. Populations decreasing from (c) to (d) is an effect of memory decay.

5 Conclusions

In this work we modelled some mechanisms that allow the *Drosophila melanogaster* in particular - and other insects in general as well - to orient in space by means of the mathematical theory of neural fields. More specifically, we proposed two different models, one for the activity of HD cells in the ellipsoid body, responsible for encoding the head direction of the animal. The second one, instead, is a network of three different populations of neurons in the protocerebral bridge, encoding not only the direction of the fly, but also storing memory of where it initially came from.

From the first model of landmark navigation, we found that with appropriate choice of parameters, the model is able to follow a visual external stimulus moving around a LED arena. Very fast oscillations of the input are damped because of the discretization of the ellipsoid body domain. We also showed that the population of HD cells was able to follow the jump of an external stimulus, for particular choices of this one. Thus, we produced a bifurcation diagram on varying width and strength of the input for different angles, showing that three outcomes are possible: one in which the bump does not follow the input at all (which is not strong enough), one where the jump is possible and the last one where the bump flows following the input without jumps. The bigger the jump (higher angles) and the strength of the input, the more the fly's brain is able to move abruptly to follow the input. For the width, instead, the model tends not to recognise jumps of inputs that are too wide.

The neural field formulation for this first model was then used to construct a more complicated network, of three populations of neurons. They cooperate to the path integration of the fly, in such a way that it is always able to retrieve the initial position after an outbound route. Our purpose was to build a model that - once the external stimulus was removed - could return back where it started. In order to obtain so, a second stimulus was defined, relying only on internally available information, instead of on external ones. This way, the returning route is made somehow linear, in the sense that even if the fly made several turns following the external input, once this one was removed it returned back without performing all the turns. This is possible because the returning process is based only on information about cumulative turns in one or the other direction.

The second model was inspired by the work of Stone et al [17], but improved with the usage of neural field. This choice was motivated by the fact that we were interested in the activity of a population of neurons as a whole, rather than on activity of single neurons. And our choice of neural field was an adaptation of Wilson-Cowan equation, allowing bump solutions, like the ones found in biological studies on insect brains. We applied an external input for some time, then once we removed it, the modelled fly was always able to return back in the correct direction, some times stopping close to

the initial position, some other times stopping before reaching it. The outcome of this experiment (reaching the exact position or not) depends on the choice of parameters, in particular the one governing the magnitude of memory decay, which in our model depends on the level activity itself.

In the paper by Stone et al. [17] some more populations of neurons were analysed, but the aim of this work was to build the simplest possible model that was still able to behave such as the fly’s brain in the real world. We managed to do so using neural fields and constructing evolutionary equations of only two populations, plus defining a variable (the steering) that was dependent on a third population, whose activity was defined as the algebraic sum of the previous two populations. This allowed us to obtain a very good model for the 1D setting. However, some information about the velocity of the fly, encoded by the TN populations in the noduli, needs to be incorporated in the model, when one wants to expand it in a 2D setting.

During the outbound route, in fact, movements in space are represented in the variables (x, y) , obtained by solving the equations

$$\begin{cases} \dot{x} = v \cos(\theta) \\ \dot{y} = v \sin(\theta) \end{cases} \quad (5.1)$$

where $v(t)$ is the velocity of the fly, and $\theta(t)$ is defined as in 4.2 as the solution to the equation $\dot{\theta} = S_i$. $S_1(t)$ is again the velocity of the external input. Once this is removed, instead, the fly is made rotating until it hits the “home direction” θ_H and then, keeping $\theta = \theta_H$ constant in 5.1, and making v dependent on internally available information, the fly is made travel until its initial position.

After the fly rotates reaching direction $\theta = \theta_H$, a new velocity v needs to be defined, and it needs to be made dependent on internally available information, in order to define a stopping criterion as well. This velocity is going to have the same role as steering in the 1D setting and here to reach the home direction. Possible improvements could be considering an additional variable modelling activity of TN neurons, which encode information about the velocity of the fly [17].

Bibliography

- [1] Shun-ichi Amari. “Dynamics of pattern formation in lateral-inhibition type neural fields”. In: *Biol. Cybern.* (1977). DOI: [10.1007/BF00337259](https://doi.org/10.1007/BF00337259).
- [2] Bard Ermentrout and Bryce J. McLeod. “Existence and uniqueness od travelling waves for a neural network”. In: *Proc. Roy. Soc. Edinburgh Sect. A* (1993). DOI: [10.1017/S030821050002583X](https://doi.org/10.1017/S030821050002583X).
- [3] G. Bard Ermentrout and David H. Terman. *Mathematical foundations of neuroscience*. Springer, 2010. DOI: [10.1007/978-0-387-87708-2](https://doi.org/10.1007/978-0-387-87708-2).
- [4] Jonathan Green, Atsuko Adachi, Kunal K Shah, et al. “A neural circuit architecture for angular integration in *Drosophila*”. In: *Nature* (2017). DOI: [10.1038/nature22343](https://doi.org/10.1038/nature22343).
- [5] Stanley Heinze and Uwe Homberg. “Maplike representation of celestial E-vector orientations in the brain of an insect”. In: *Science* (2007). DOI: [10.1126/science.1135531](https://doi.org/10.1126/science.1135531).
- [6] Sung Soo Kim, Hervé Roualt, Shaul Druckmann, et al. “Ring attractor dynamics in the *Drosophila* central brain”. In: *Science* (2017). DOI: [10.1126/science.aal4835](https://doi.org/10.1126/science.aal4835).
- [7] Kengo Kishimoto and Shum-ichi Amari. “Existence and stability of local excitations in homogeneous neural fields”. In: *J Math Biol.* (1979). DOI: [10.1007/BF00275151](https://doi.org/10.1007/BF00275151).
- [8] Joshoua P. Martin, Guo Peiyuan, Laiyong Mu, et al. “Central-complex control of movement in the freely walking cockroach”. In: *Curr. Biol.* (2015). DOI: [10.1016/j.cub.2015.09.044](https://doi.org/10.1016/j.cub.2015.09.044).
- [9] Bruce L. McNaughton, Francesco P. Battaglia, Ole Jensen, et al. “Path integration and the neural basis of the cognitive map”. In: *Nat Rev Neurosci.* (2006). DOI: [10.1038/nrn1932](https://doi.org/10.1038/nrn1932).
- [10] Jaison Jiro Omoto, Bao-Chau Minh Nguyen, Pratyush Kandimalla, et al. “Neuronal constituents and putative interactions within the *Drosophila* ellipsoid body neuropil”. In: *Frontiers in Neural Circuit* (2018). DOI: [10.3389/fncir.2018.00103](https://doi.org/10.3389/fncir.2018.00103).
- [11] Sara M. Park Emily J.and Wasserman. “Diversity of visuomotor reflexes in two *Drosophila* species”. In: *Curr. Biol.* (2018). DOI: [10.1016/j.cub.2018.06.071](https://doi.org/10.1016/j.cub.2018.06.071).
- [12] Adrien Peyrache, Marie M. Lacroix, Peter Petersen, et al. “Internally-organized mechanisms of the head direction sense”. In: *Nat. Neurosci.* (2015). DOI: [10.1038/nn.3968](https://doi.org/10.1038/nn.3968).

- [13] David J. Pinto and G. Bard Ermentrout. “Spatially structured activity in synaptically coupled neuronal networks: I. Travelling fronts and pulses”. In: (2001). DOI: [10.1137/S0036139900346453](https://doi.org/10.1137/S0036139900346453).
- [14] Johannes D. Seelig and Vivek Jayaraman. “Neural dynamics for landmark orientation and angular path integration”. In: *Nature* (2015). DOI: [10.1038/nature14446](https://doi.org/10.1038/nature14446).
- [15] Patricia E. Sharp, Hugh T. Blair, and Jeiwon Cho. “The anatomical and computational basis of the rat head-direction cell signal”. In: *Trends Neurosci.* (2001). DOI: [10.1016/s0166-2236\(00\)01797-5](https://doi.org/10.1016/s0166-2236(00)01797-5).
- [16] Pengcheng Song and Xiao-Jing Wang. “Angular Path Integration by Moving “Hill of Activity”: A Spiking Neuron Model without Recurrent Excitation of the Head-Direction System”. In: *J. Neurosci.* (2005). DOI: [10.1523/JNEUROSCI.4172-04.2005](https://doi.org/10.1523/JNEUROSCI.4172-04.2005).
- [17] Thomas Stone, Barbara Webb, Andrea Adden, et al. “An anatomically constrained model for path integration in the bee brain”. In: *Current Biology* (2017). DOI: [10.1016/j.cub.2017.08.052](https://doi.org/10.1016/j.cub.2017.08.052).
- [18] Luis F. Sullivan, Timothy L. Warren, and Chris Q. Doe. “Temporal identity establishes columnar neuron morphology, connectivity, and function in a *Drosophila* navigation circuit”. In: *eLife* (2019). DOI: [10.7554/eLife.43482](https://doi.org/10.7554/eLife.43482).
- [19] Peter Tass. “Cortical pattern formation during visual hallucinations”. In: *J Biol Phys* (1995). DOI: [10.1007/BF00712345](https://doi.org/10.1007/BF00712345).
- [20] Jeffrey S. Taube. “The Head Direction Signal: Origins and Sensory-Motor Integration”. In: *Annu Rev Neurosci.* (2007). DOI: [10.1146/annurev.neuro.29.051605.112854](https://doi.org/10.1146/annurev.neuro.29.051605.112854).
- [21] Jeffrey S. Taube, Robert U. Muller, and James B. jr Ranck. “Head-Direction Cells Recorded from the Postsubiculum in Freely Moving Rats. I. Description and Quantitative Analysis”. In: *J. Neurosci.* (1990). DOI: [10.1523/JNEUROSCI.10-02-00420.1990](https://doi.org/10.1523/JNEUROSCI.10-02-00420.1990).
- [22] Daniel Turner-Evans, Stephanie Wegener, Hervé Rouault, et al. “Angular velocity integration in a fly heading circuit”. In: *eLife* (2017). DOI: [10.7554/eLife.23496](https://doi.org/10.7554/eLife.23496).
- [23] Hugh R. Wilson and Jack D. Cowan. “Excitatory and inhibitory interactions in localized populations of model neurons”. In: *Biophys. J.* (1972). DOI: [10.1016/S0006-3495\(72\)86068-5](https://doi.org/10.1016/S0006-3495(72)86068-5).
- [24] Kechen Zhang. “Representation of Spatial Orientation by the Intrinsic Dynamics of the Head-Direction Cell Ensemble: A Theory”. In: *J. Neurosci.* (1996). DOI: [10.1523/JNEUROSCI.16-06-02112.1996](https://doi.org/10.1523/JNEUROSCI.16-06-02112.1996).